



# Understanding the relationship between atomic structures and transport properties in $(\text{Cu}_{0.5}\text{Zr}_{0.5})_{100-x}\text{Al}_x$ ( $x \leq 10$ ) glass forming liquids: Molecular dynamics simulations

Y. Zhang<sup>a,\*</sup>, N. Mattern<sup>a</sup>, J. Eckert<sup>a,b</sup>

<sup>a</sup> IFW Dresden, Institute for Complex Materials, Helmholtzstr. 20, D-01069 Dresden, Germany

<sup>b</sup> TU Dresden, Institute of Materials Science, D-01062 Dresden, Germany

## ARTICLE INFO

### Article history:

Received 19 August 2011

Received in revised form 5 November 2011

Accepted 7 November 2011

Available online 23 November 2011

### Keywords:

Metallic glasses

Atomic structure

Glass-forming ability

Diffusion

## ABSTRACT

We have performed a systematic investigation on the atomic structures, thermal and transport properties of  $(\text{Cu}_{0.5}\text{Zr}_{0.5})_{100-x}\text{Al}_x$  ( $x \leq 10$ ) glass forming liquids using MD simulations, aiming to underpin the understanding of the relationship between atomic structures and the experimentally observed glass forming ability in the system. A good correlation between the atomic structures and the transport properties has been revealed. Macroscopically, it is found that the composition with  $x=7$  has the highest viscosity and the lowest diffusivity near the glass transition, which are responsible for the best glass forming around  $x=7$  or 8 observed experimentally. At the atomic scale, the short range order of both glass forming liquids and the resultant glasses shows a strong dependence on Al additions. By a careful analysis of the chemical environment of the icosahedra and icosahedra-like clusters, we categorize the sub-types of these clusters into three groups according to their behaviors upon Al additions. The sub-types in group III show an excellent correlation between the transport properties and the glass forming ability. We propose that such clusters can govern the transport properties and glass forming ability in  $(\text{Cu}_{0.5}\text{Zr}_{0.5})_{100-x}\text{Al}_x$  glass-forming liquids within the studied composition range.

© 2011 Elsevier B.V. All rights reserved.

## 1. Introduction

Bulk metallic glasses (BMGs) have received enormous attention of materials scientists and physicists during the past decades [1]. Firstly, BMGs possess ultrahigh strengths and outstanding elasticity [2], which are very promising as new structural materials. Secondly, many fundamental questions remain open in BMGs [3] despite numerous models have been proposed, such as their atomic structure [4,5] and the relationships between structure and glass transition [6], glass forming ability (GFA) [7,8] and plasticity [9,10]. It is earlier believed that the BMG-forming alloys favor multi-component systems which are close to the eutectic points [11]. However, the discovery of many binary BMGs at many off-eutectic compositions challenges our understanding towards GFA [12,13]. For example,  $\text{Cu}_{50}\text{Zr}_{50}$ , which is an “intermetallic glass” with the stoichiometry of CuZr B2 phase, can be prepared into BMGs with a critical diameter of 1–2 mm [14]. The addition of Al can significantly enhance the GFA of the Cu–Zr BMGs [15]. So far, the best GFA in Cu–Zr–Al system is achieved in  $\text{Zr}_{45}\text{Cu}_{47}\text{Al}_8$  with a critical diameter of 15 mm [16].

Using  $\text{Cu}_{50}\text{Zr}_{50}$  as a master alloy,  $(\text{Cu}_{0.5}\text{Zr}_{0.5})_{100-x}\text{Al}_x$  ( $x \leq 10$ ) BMGs have been developed and their thermal and mechanical properties have been intensively studied. The best GFA in  $(\text{Cu}_{0.5}\text{Zr}_{0.5})_{100-x}\text{Al}_x$  BMGs is found at  $x=8$  at% with a critical diameter of at least 5 mm [17]. Although the  $(\text{Cu}_{0.5}\text{Zr}_{0.5})_{100-x}\text{Al}_x$  BMGs do not possess the best GFA, they show very attractive mechanical properties. A large compressive strain up to 18% has been observed in a  $(\text{Cu}_{0.5}\text{Zr}_{0.5})_{95}\text{Al}_5$  BMG with a pronounced “work-hardening” effect induced by the interactions of multiple shear bands [18]. It is suggested that large Poisson’s ratios may indicate ductile BMGs. Accordingly, the Poisson’s ratio is found to reach a maximum at the compositions around  $x=4-5$  [19,20]. The most charming feature of  $(\text{Cu}_{0.5}\text{Zr}_{0.5})_{100-x}\text{Al}_x$  BMGs is their uncommon ductility under tension at room temperature [21]. Moreover, BMG composites with various microstructures can be prepared by careful controlling of cooling rates, some of which show a transformation mediated ductility under tension [22].

Many experimental and theoretical studies have been carried out to investigate the structures of Cu–Zr–Al BMGs. Diffraction measurements show that the structure of Cu–Zr BMGs can be modeled by an ideal solution approximation because of the relatively weak Cu–Zr interactions (heat of mixing  $\Delta H_{\text{mix}} = -23$  kJ/mol). However, the structures of Cu–Zr–Al BMGs deviate from the ideal solution approximation remarkably due to the strong interactions

\* Corresponding author. Tel.: +49 351 4659 686; fax: +49 351 4659 452.

E-mail address: [yue.zhang@ifw-dresden.de](mailto:yue.zhang@ifw-dresden.de) (Y. Zhang).

of Zr–Al ( $\Delta H_{\text{mix}} = -44$  kJ/mol), leading to a large number of Zr–Al nearest neighbors with high packing efficiency and an enhanced GFA as a consequence [23]. At the meanwhile, investigations on the structures of  $(\text{Cu}_{0.5}\text{Zr}_{0.5})_{92}\text{Al}_8$  [24],  $\text{Cu}_{46}\text{Al}_{47}\text{Al}_7$  [25] and  $\text{Zr}_{48}\text{Cu}_{45}\text{Al}_7$  [26] BMGs have been investigated using molecular dynamics (MD) simulations and reverse Monte Carlo simulations, respectively. The results suggest a remarkable network of icosahedra (ICO) type short range order (SRO) in these glasses. However, a systematic investigation of the impact of Al additions on the atomic structures of  $(\text{Cu}_{0.5}\text{Zr}_{0.5})_{100-x}\text{Al}_x$  metallic glasses (MGs) and liquids is still lacking. Besides structural aspects, transport properties such as diffusivity and viscosity also constitute important factors in the competition between crystallization and glass formation. Nevertheless, the relationship between the atomic structures and the transport properties in  $(\text{Cu}_{0.5}\text{Zr}_{0.5})_{100-x}\text{Al}_x$  system remains poorly understood due to the experimental difficulties to handle metastable metallic supercooled liquids within the experimental time window.

In this study, we perform a systematic investigation on the atomic structures, thermal and transport properties of  $(\text{Cu}_{0.5}\text{Zr}_{0.5})_{100-x}\text{Al}_x$  glass forming liquids and glasses with various Al additions using MD simulations. MD simulations are very powerful to overcome the instability of supercooled liquids against crystallization. Al addition is found to significantly influence the SRO and transport properties of  $(\text{Cu}_{0.5}\text{Zr}_{0.5})_{100-x}\text{Al}_x$  liquids near glass transition. The best GFA around  $x=7$  or 8 observed experimentally is revealed to be closely related with some special SROs, which sheds a light to a deeper understanding of the relationship between atomic structures and GFA.

## 2. Methods

### 2.1. Simulation process

Classical MD simulations were conducted to study the atomic structures and transport properties of  $(\text{Cu}_{0.5}\text{Zr}_{0.5})_{100-x}\text{Al}_x$  glass forming liquids with  $x=0, 2, 5, 7$  and 10, respectively. The atomic interactions were described by the potential produced by Sheng et al. [25] using the embedded atom method (EAM). Cubic simulation boxes containing 51,200 atoms were constructed by randomly arranging Cu, Zr and Al boxes according to the stoichiometry. Periodic boundary conditions were applied throughout the whole simulation process. The time interval for integration was set to be 2.5 fs.

We employ *NPT* ensemble (constant number of atoms, pressure and temperature) using a Nosé–Hoover thermostat for temperature control [27]. All the initial configurations were held at 2000 K for 10 ns, which is about 800 K higher than the liquidus temperatures of these alloys. The holding time of 10 ns at 2000 K is long enough for the structures to reach equilibrium states, so that all the structures obtained in subsequent simulations are independent of the initial configurations. Then, the systems were cooled from 2000 to 300 K using a “cooling–holding” approach, i.e. after cooled for each temperature interval of 100 K at 1 K/ps, the system was isothermally relaxed for 100 ps before the next cooling took place. The external pressure was set to zero. The atomic structures, thermal and transport properties were calculated using the atomic trajectories collected under *NVT* ensemble (constant number of atoms, volume and temperature), viz., after each holding for 100 ps under *NPT* in the “cooling–holding” approach, an independent simulation for sampling was carried out for 1–10 ns (depends on temperature) under *NVT*. We believe that such procedure can effectively relax the structures and eliminate the impact of the box vibration on the Voronoi tessellation.

### 2.2. Structural analysis

Atomic structures of the simulated  $(\text{Cu}_{0.5}\text{Zr}_{0.5})_{100-x}\text{Al}_x$  MGs and liquids were characterized by both pair correlation functions (PCFs) and the Voronoi tessellation. The total PCFs,  $g(r)$ , was defined as:

$$g(r) = \frac{V}{N^2} \left\langle \sum_{i=1}^N \frac{n_i(r)}{4\pi r^2 \Delta r} \right\rangle \quad (1)$$

where  $N$  is the total number of atoms in simulation cell,  $V$  is the volume and  $n_i(r)$  the number of atoms which can be found in the shell from  $r$  to  $r + \Delta r$ . Partial PCFs for atom type  $\alpha$  and  $\beta$  are defined by:

$$g_{\alpha\beta}(r) = \frac{V}{N_\alpha N_\beta} \left\langle \sum_{i=1}^{N_\alpha} \frac{n_i(r)}{4\pi r^2 \Delta r} \right\rangle \quad (2)$$

where  $N_\alpha$  and  $N_\beta$  are the number of type  $\alpha$  and  $\beta$  atoms, respectively. For Voronoi tessellation, we averaged the results of the Voronoi tessellation of 50 atomic configurations in order to have a reliable statistics. The difference in the atomic radii was taken into account during the construction of the Voronoi polyhedra (VP). We also deleted very small facets with areas of less than 0.5% of the total area of the VP to minimize the thermal effect [4].

### 2.3. Thermal and transport properties

The thermal expansion coefficients (TECs) and isobaric heat capacities ( $C_p$ ) were calculated based on the evolution of the box length and the enthalpy of the system using the following equations, respectively:

$$\alpha = \frac{1}{L} \frac{dL}{dT} \quad (3)$$

$$C_p = \left( \frac{\partial H}{\partial T} \right)_p \quad (4)$$

where  $\alpha$ ,  $L$  and  $H$  are the TEC, box length and enthalpy, respectively.

The self-diffusion coefficients  $D(T)$  were calculated using the long-time evolution of the mean square displacements (MSDs) by the following equations:

$$\langle r^2(t) \rangle = \frac{1}{N} \sum_{i=1}^N \langle |r_i(t) - r_{i0}(t)|^2 \rangle \quad (5)$$

$$D(T) = \lim_{t \rightarrow \infty} \frac{1}{6} \frac{\partial \langle r^2(t) \rangle}{\partial t} \quad (6)$$

where  $r_i(t)$  is the atomic position at time  $t$  and  $\langle \rangle$  denotes an ensemble average. We employed the equilibrium MD (EMD) method based on the shear auto-correlation function to calculate the shear viscosity using the following equation:

$$\eta = \frac{V}{NkT} \int_0^\infty \left\langle \sum_{i=1}^N P_i(0)P_i(t) \right\rangle dt \quad (7)$$

where  $\eta$  denotes the shear viscosity,  $V$  is the volume of the simulation box,  $N$  is the total number of atoms in the system box and  $k$  is the Boltzmann constant.  $P_i(t)$  denotes the off-diagonal components of the atomic stress tensor at time  $t$  and  $\langle \rangle$  represents an ensemble average.

## 3. Results and discussion

### 3.1. Heat capacity, thermal expansion and glass transition

The evolution of the potential energy (PE) of the simulated  $(\text{Cu}_{0.5}\text{Zr}_{0.5})_{100-x}\text{Al}_x$  systems as a function of temperature during cooling is illustrated in Fig. 1. PE of all the systems decreases smoothly during cooling, where no abrupt changes in PE associated with crystallization can be observed. The apparent glass transition temperature ( $T_g$ ) is determined by extrapolating and intersecting the two linear parts of PE curves from 300 to 900 K. It can be seen that  $\text{Cu}_{50}\text{Zr}_{50}$  MG has the lowest  $T_g$  of 724.7 K.  $T_g$  increases with Al addition (see inset of Fig. 1), which is consistent with the experimental results [17,20]. However,  $T_g$  values determined by MD simulations are about 50 K higher than experimental results. The discrepancy between MD simulations and experiments is probably due to (1) ultrahigh cooling rates used in MD simulations and (2) different procedures used to evaluate  $T_g$  (MD: cooling, experiments: heating).

The TECs and  $C_p$  of the simulated  $(\text{Cu}_{0.5}\text{Zr}_{0.5})_{100-x}\text{Al}_x$  MGs and liquids in the temperature range of 2000–300 K are shown in Fig. 2(a) and (b), respectively. Glass transition takes place in all the investigated compositions during cooling, which can be clearly reflected by a jump on both TEC and  $C_p$  curves in the temperature range from 700 to 1100 K.  $C_p$  of  $(\text{Cu}_{0.5}\text{Zr}_{0.5})_{100-x}\text{Al}_x$  liquids is

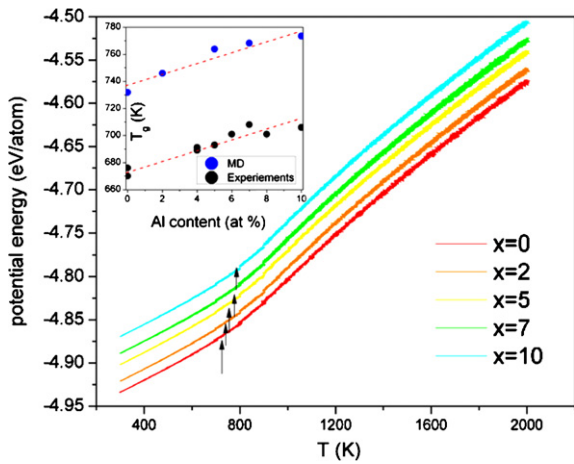


**Fig. 1.** The potential energy of the simulated  $(\text{Cu}_{0.5}\text{Zr}_{0.5})_{100-x}\text{Al}_x$  systems during cooling. The inset shows the glass transition temperatures obtained by simulations and experiments (Ref. [17]).

insensitive to Al addition from 2000 to 1100 K. However, the overshooting of  $C_p$  increases with Al addition from 1100 to 900 K in the supercooled liquid regime. After glass transition, the  $C_p$  values of the resultant MGs are found to be quite identical. The TECs of  $(\text{Cu}_{0.5}\text{Zr}_{0.5})_{100-x}\text{Al}_x$  liquids increase upon Al addition more significantly than  $C_p$ . It can be seen that the TEC of all the investigated compositions are almost constant in the temperature range from 2000 to 1400 K. Upon further cooling from 1400 to 900 K, the TEC exhibits an increase of about 4.5%, followed by a remarkable decrease of about 50% upon glass transition between 700 and 900 K. The calculated TEC and  $C_p$  values in this work are in good agreement with the experimental values of some Zr-based glass-forming liquids and glasses [28,29].

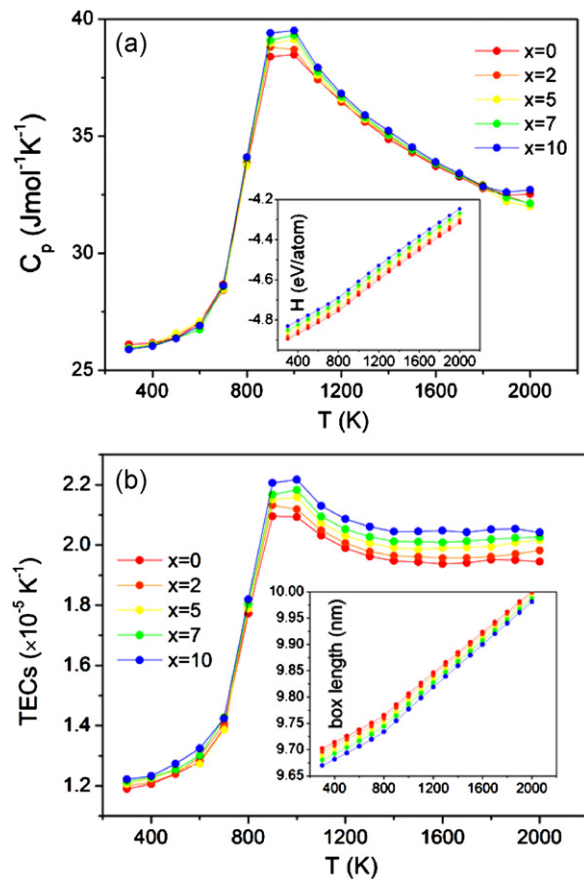


**Fig. 2.** The  $C_p$  (a) and TECs (b) of the simulated  $(\text{Cu}_{0.5}\text{Zr}_{0.5})_{100-x}\text{Al}_x$  MGs and liquids in the temperature range of 2000–300 K, respectively. The insets of (a) and (b) are the evolutions of box lengths and enthalpy as a function of temperature, respectively.

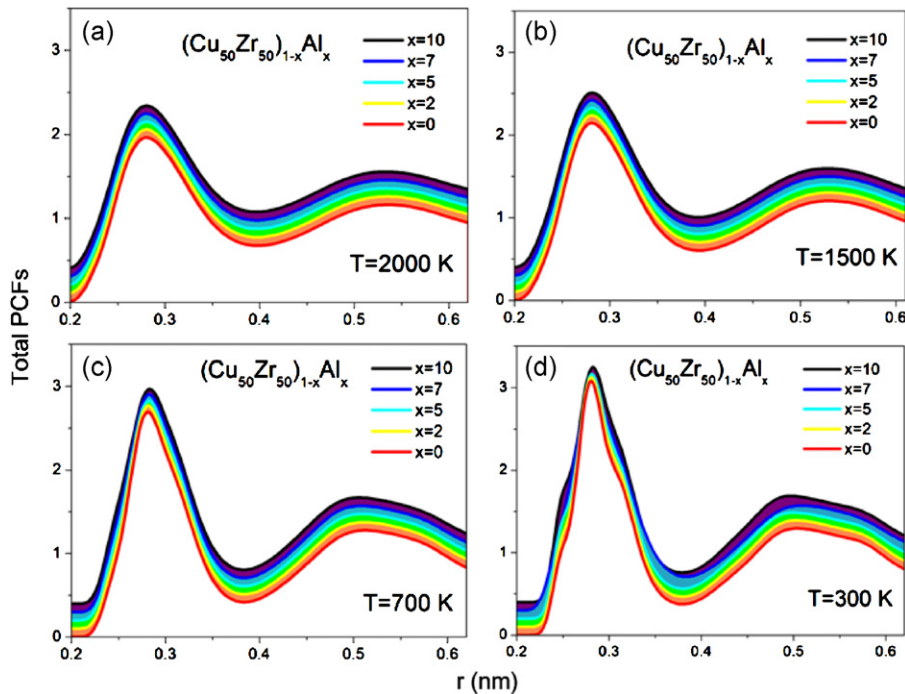


**Fig. 3.** The total PCFs of the simulated  $(\text{Cu}_{0.5}\text{Zr}_{0.5})_{100-x}\text{Al}_x$  MGs and liquids at 2000, 1500, 700 and 300 K, respectively. An offset of 0.1 on y-axis is applied for clarity.

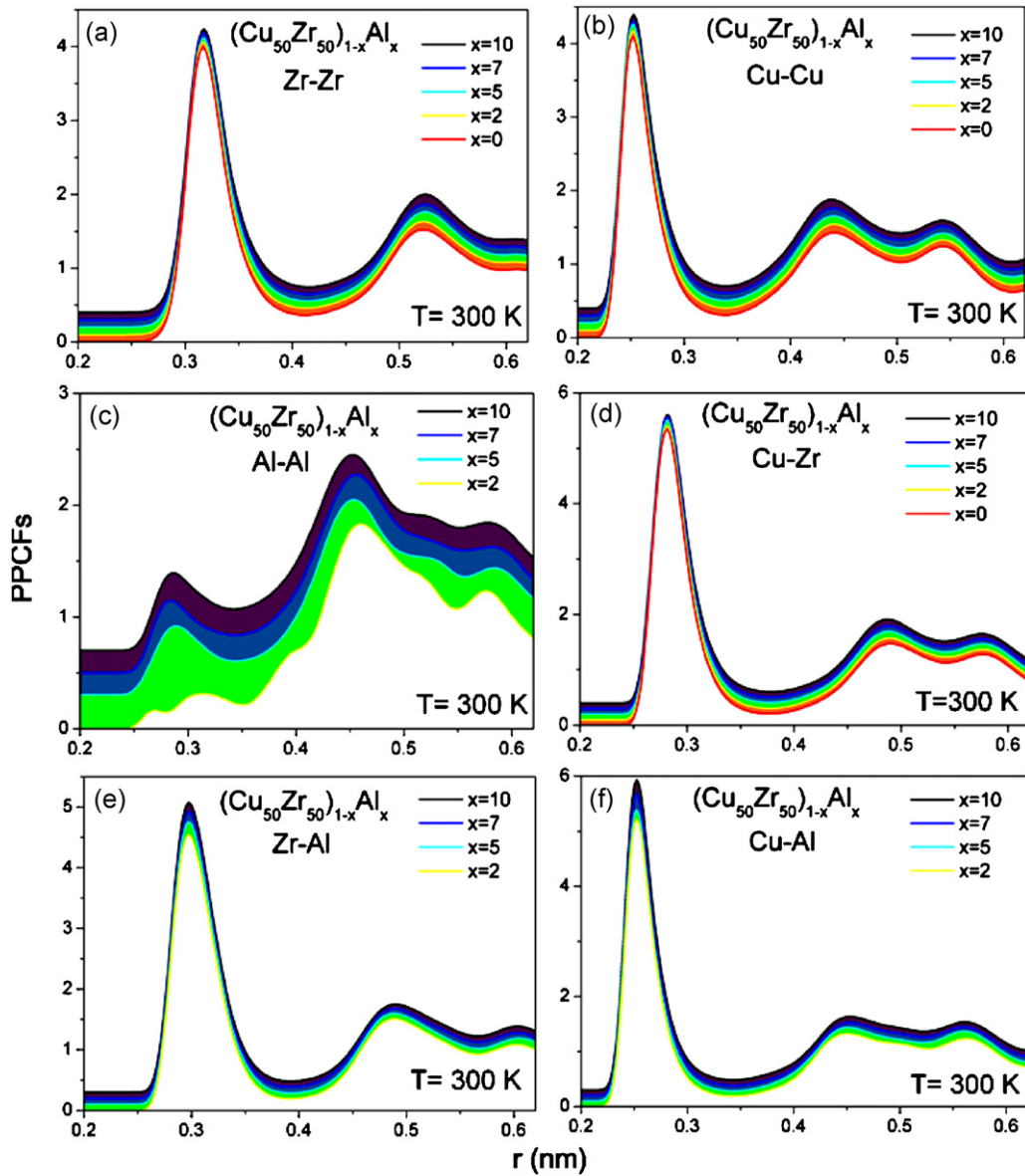


Fig. 4. The partial PCFs of the simulated  $(\text{Cu}_{0.5}\text{Zr}_{0.5})_{100-x}\text{Al}_x$  MGs at 300 K.

## 3.2. Atomic structures

### 3.2.1. Pair correlation functions

The total PCFs of the simulated  $(\text{Cu}_{0.5}\text{Zr}_{0.5})_{100-x}\text{Al}_x$  MGs and liquids at 2000, 1500, 700 and 300 K are presented in Fig. 3(a)–(d), respectively. The four temperatures are chosen as they are representative for initial state (2000 K), equilibrium liquids (1500 K), glass transition (700 K) and glassy state (300 K), respectively. It can be seen that all the total PCFs exhibit typical features of either liquids or glasses, where a periodically translational long range order is absent. Upon cooling, the amplitudes of both the first and second maxima of the total PCFs increase while their widths decrease, which is due to the formation of a higher degree of SRO with enhanced stability in glasses compared to liquids. It is hard to distinguish the effect of Al addition on the total PCFs above glass transition within the investigated composition range. However, two humps on the first maximum can be observed below glass transition. The amplitudes of both humps increase upon Al addition, which becomes more pronounced upon further cooling from 700 to 300 K, as shown in Fig. 3(d). The hump after the first maximum is

commonly observed in CuZr-based BMGs [30,31], which is believed to be related with some preferential types of SRO built around Zr atoms. However, the hump before the first maximum usually cannot be observed experimentally. Thus, we deduce that it is either associated with the employed potential or with some preferential types of SROs under ultrahigh cooling rates used in MD simulations.

In order to evaluate the impact of Al addition on the atomic structures, we plot all the partial PCFs of  $(\text{Cu}_{0.5}\text{Zr}_{0.5})_{100-x}\text{Al}_x$  MGs at 300 K in Fig. 4. The relationship between the total and partial PCFs can be described by the following equation:

$$g(r) = \sum_{\alpha=\beta} W_{\alpha\beta} g_{\alpha\beta}(r) + 2 \sum_{\alpha \neq \beta} W_{\alpha\beta} g_{\alpha\beta}(r) \quad (8)$$

where  $W_{\alpha\beta} = c_{\alpha}c_{\beta}F_{\alpha}F_{\beta}/(\sum c_i F_i)^2$ ,  $c_i$  is the atomic concentration and  $F_i$  is the atomic form factor. The weighting factors  $W_{ij}$  of  $(\text{Cu}_{0.5}\text{Zr}_{0.5})_{100-x}\text{Al}_x$  metallic glasses are listed in Table 1. It can be seen that the Cu–Cu, Zr–Zr and Cu–Zr atomic pairs contribute to the most of the total PCFs. Upon Al addition, the contributions

of Al–Al, Al–Cu and Al–Zr pairs increase but their sum is still below 10%. All the partial PCFs show similar behaviors like the total PCFs except the Al–Al pair. The first maximum of Al–Al partial PCF shows a splitting at the Al addition of 2 at%, which may arise from some preferred Al–Cu and Al–Zr clustering under very low Al concentrations. It becomes a single peak as the Al concentration is higher than 5 at%. Although the amplitudes of the first maximum increase upon Al addition, the first maxima are still below unity, indicating that the clustering of Al–Al atoms is not favored as Al addition is below 10 at%. The separation of Al atoms can be understood in terms of  $\Delta H_{\text{mix}}$ , which is one of the most important factors governing the GFA. Due to the highly negative values of  $\Delta H_{\text{mix}}$  of Zr–Al ( $-44$  kJ/mol) and Zr–Cu ( $-23$  kJ/mol), Al atoms are preferentially bonded with Zr atoms. However, formations of Zr–Cu bonds and Zr–Al bonds compete with each other since there is a much larger population of Cu atoms in the system. Consequently, the amplitudes of the first maxima of the Zr–Cu and Zr–Al partial PCFs are comparable. Although the negligible  $\Delta H_{\text{mix}}$  of Cu–Al ( $-1$  kJ/mol) provides almost equal chances to form Cu–Al and Al–Al bonds, the overwhelming number of Cu atoms makes the formation of Cu–Al bonds more favorable, contributing further to the separation of Al atoms.

### 3.2.2. Voronoi tessellation

The fractions of predominant VP types in  $(\text{Cu}_{0.5}\text{Zr}_{0.5})_{100-x}\text{Al}_x$  metallic glasses and liquids are presented in Fig. 5. In order to have a direct comparison, we normalized the fractions of VPs with respect to the atomic concentrations. A VP type is chosen as a predominant type if its fraction has ever been larger than 2% during cooling from 2000 to 300 K. It can be seen that the most frequent VPs centered by Zr atoms are ICO-like [32], such as  $\langle 01103 \rangle$ ,  $\langle 01104 \rangle$ ,  $\langle 0284 \rangle$ ,  $\langle 0285 \rangle$  and  $\langle 0286 \rangle$ . Among these clusters,  $\langle 01104 \rangle$  and  $\langle 0285 \rangle$  clusters have the largest populations in the resultant MGs at 300 K, corresponding to about 6% and 5%, respectively. However, the most popular VPs centered by Cu or Al atoms are full ICO clusters with an index of  $\langle 00120 \rangle$ . It can be clearly seen that Al atoms have the strongest tendency to build full ICO clusters around them, taking into account that the number of Al atoms is 10–25 times smaller than that of Cu atoms in the simulation boxes. Besides the full ICO, there are also abundant ICO-like clusters, such as the Cu-centered  $\langle 0281 \rangle$  and  $\langle 0282 \rangle$  and Al-centered  $\langle 01102 \rangle$ . The fractions of both full ICO and ICO-like VPs increase dramatically in the vicinity of glass transition. Previous studies have shown that the Cu-centered  $\langle 00120 \rangle$ ,  $\langle 0282 \rangle$  and Zr-centered  $\langle 01104 \rangle$  clusters have the slowest dynamics in Cu–Zr liquids [32,33], which correlate with the GFA very well. We believe that the total fractions of ICO and ICO-like clusters can be a good indicator to evaluate the GFA of glass-forming liquids. It can be seen that the total fractions of ICO and ICO-like clusters centered by Zr- and Cu atoms show a maximum at  $x=7$ , which is in good agreement with the best GFA at  $x=8$  observed experimentally. Moreover, both the Cu- and Al-centered ICO cluster in  $(\text{Cu}_{0.5}\text{Zr}_{0.5})_{100-x}\text{Al}_x$  MGs have maxima at  $x=7$  at 300 K, indicating a more densely packed atomic structure as a consequence of the best GFA. The total fractions of Al-centered common VPs show a maximum at  $x=5$ . However, the contribution

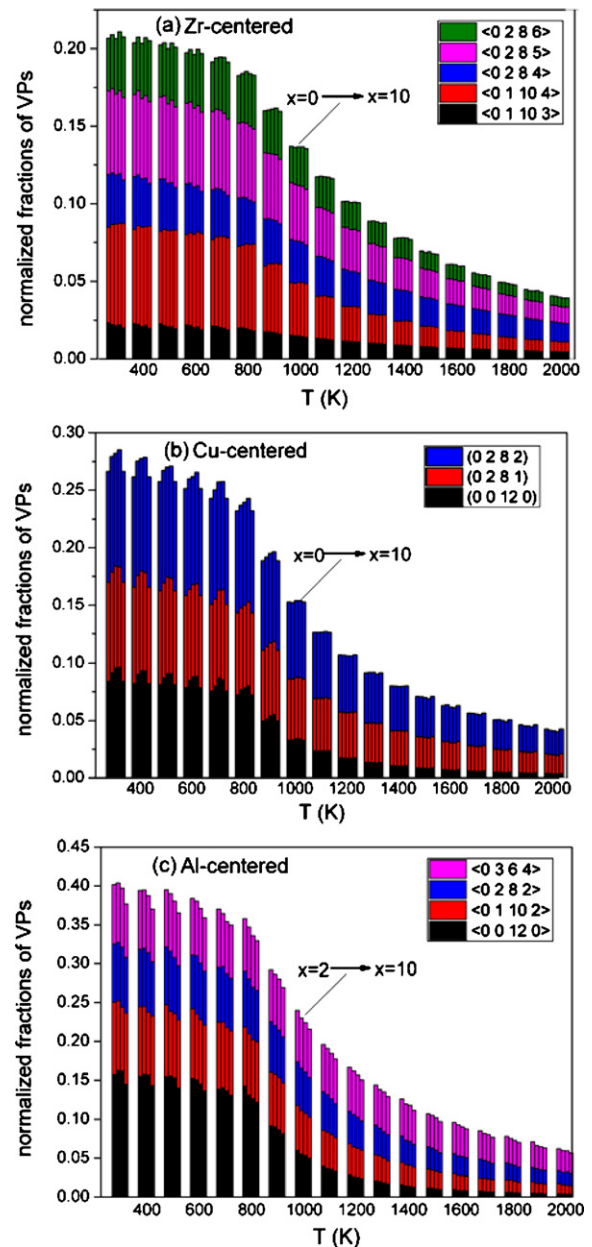


Fig. 5. The evolution of major VP types of the simulated  $(\text{Cu}_{0.5}\text{Zr}_{0.5})_{100-x}\text{Al}_x$  MGs during cooling centered by (a) Zr, (b) Cu and (c) Al atoms, respectively.

of Al-centered VPs will not change the overall trend of Zr- and Cu-centered clusters due to their low concentrations.

In order to yield detailed information on atomic structures, we further analyze the local chemistry (sub-types) of the above mentioned predominant VP types in  $(\text{Cu}_{0.5}\text{Zr}_{0.5})_{100-x}\text{Al}_x$  MGs at 300 K. We only focus on the sub-types whose fractions have ever been larger than 5% among all the studied compositions. The sub-types of Zr-centered  $\langle 0286 \rangle$  are presented in Fig. 6 as an

Table 1

The weighting factors of the partial PCFs of  $(\text{Cu}_{0.5}\text{Zr}_{0.5})_{100-x}\text{Al}_x$  MGs at 300 K.

	$W_{\text{Zr-Zr}}$	$W_{\text{Cu-Cu}}$	$W_{\text{Al-Al}}$	$2W_{\text{Cu-Zr}}$	$2W_{\text{Cu-Al}}$	$2W_{\text{Zr-Al}}$
$\text{Cu}_{50}\text{Zr}_{50}$	0.3363	0.1765	–	0.4872	–	–
$(\text{Cu}_{0.5}\text{Zr}_{0.5})_{98}\text{Al}_2$	0.3312	0.1738	$5.8095\text{E}-5$	0.4798	0.0064	0.0088
$(\text{Cu}_{0.5}\text{Zr}_{0.5})_{95}\text{Al}_5$	0.3234	0.1697	$3.7725\text{E}-4$	0.4685	0.0160	0.0221
$(\text{Cu}_{0.5}\text{Zr}_{0.5})_{93}\text{Al}_7$	0.3180	0.1669	$7.5883\text{E}-4$	0.4608	0.0225	0.0311
$(\text{Cu}_{0.5}\text{Zr}_{0.5})_{90}\text{Al}_{10}$	0.3098	0.1626	0.0016	0.4489	0.0324	0.0447

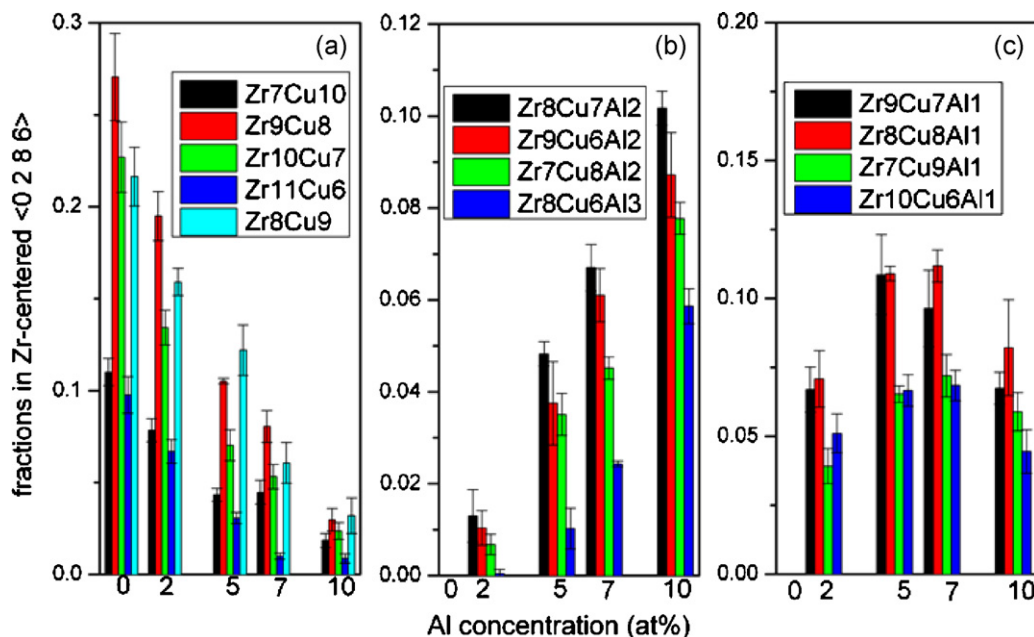


Fig. 6. Fractions of sub-types of the Zr-centered  $\langle 0286 \rangle$  in the simulated  $(\text{Cu}_{0.5}\text{Zr}_{0.5})_{100-x}\text{Al}_x$  MGs at 300 K, (a), (b) and (c) correspond to group I, II and III, respectively.

example. For clarity, we listed the sub-types of all the other Zr-, Cu- and Al-centered VPs in Tables 2–4, respectively. The error bars were obtained by averaging the results of Voronoi tessellation of at least 50 configurations collected during the NVT relaxation. From Table 4, it can be directly seen that the chemical environment of Al atoms is Zr-rich, indicating a strong alloying effect. The sub-types of the Zr-centered  $\langle 0286 \rangle$  can be categorized into three groups, corresponding to Fig. 6(a)–(c), respectively. It can be seen that the major sub-types of Zr-centered  $\langle 0286 \rangle$  in  $\text{Cu}_{50}\text{Zr}_{50}$  MG are  $\text{Zr}_9\text{Cu}_8$  (27%),  $\text{Zr}_{10}\text{Cu}_7$  (23%),  $\text{Zr}_8\text{Cu}_9$  (22%),  $\text{Zr}_7\text{Cu}_{10}$  (11%) and  $\text{Zr}_{11}\text{Cu}_6$  (10%) at 300 K, respectively. We name these sub-types as group I. The fractions of group I sub-types decrease monotonously upon Al addition, which is a result of the substitution of Zr and Cu atoms by Al atoms. Different group I sub-types show quite different stabilities against Al addition. The  $\text{Zr}_7\text{Cu}_{10}$  sub-type shows the highest

stability upon Al addition in  $(\text{Cu}_{0.5}\text{Zr}_{0.5})_{100-x}\text{Al}_x$  MGs, whose fraction in  $x = 10$  remains about 16.8% of that in  $x = 0$  at 300 K. Whereas the  $\text{Zr}_{11}\text{Cu}_6$  sub-type shows the poorest stability, whose fraction in  $x = 10$  preserves only 8.3% of that in  $x = 0$ . As a consequence of the decrease in the fractions of type I sub-types, some ternary sub-types increase with Al addition (group II), which are mainly clusters with two or three Al atoms in the local environment, such as  $\text{Zr}_8\text{Cu}_7\text{Al}_2$ ,  $\text{Zr}_9\text{Cu}_6\text{Al}_2$ ,  $\text{Zr}_7\text{Cu}_8\text{Al}_2$  and  $\text{Zr}_8\text{Cu}_6\text{Al}_3$  as shown in Fig. 6(b). Interestingly, we have also identified some ternary sub-types (group III) which show maxima around  $x = 5$ –7. Such ternary sub-types are mainly with only one substitutive Al atom, such as  $\text{Zr}_9\text{Cu}_7\text{Al}_1$ ,  $\text{Zr}_8\text{Cu}_8\text{Al}_1$ ,  $\text{Zr}_7\text{Cu}_9\text{Al}_1$  and  $\text{Zr}_{10}\text{Cu}_6\text{Al}_1$ . Besides these four sub-types in Zr-centered  $\langle 0286 \rangle$ , the  $\text{Zr}_8\text{Cu}_7\text{Al}_1$ ,  $\text{Zr}_9\text{Cu}_6\text{Al}_1$  and  $\text{Zr}_{10}\text{Cu}_5\text{Al}_1$  in Zr-centered  $\langle 01104 \rangle$ , the  $\text{Zr}_8\text{Cu}_7\text{Al}_1$ ,  $\text{Zr}_9\text{Cu}_6\text{Al}_1$ ,  $\text{Zr}_7\text{Cu}_8\text{Al}_1$  and  $\text{Zr}_{10}\text{Cu}_5\text{Al}_1$  in Zr-centered  $\langle 0285 \rangle$ , the  $\text{Zr}_7\text{Cu}_5\text{Al}_1$  in

Table 2  
Sub-types of Zr-centered  $\langle 01104 \rangle$  and  $\langle 0285 \rangle$  in the simulated  $(\text{Cu}_{0.5}\text{Zr}_{0.5})_{100-x}\text{Al}_x$  MGs at 300 K.

VP type	Sub-type	$x=0$	$x=2$	$x=5$	$x=7$	$x=10$
Zr-centered $\langle 01104 \rangle$	$\text{Zr}_9\text{Cu}_7$	0.30/0.01	0.20/0.01	0.12/0.01	0.08/0.001	0.04/0.001
	$\text{Zr}_{11}\text{Cu}_5$	0.10/0.01	0.08/0.01	0.04/0.001	0.02/0.002	0.007/0.002
	$\text{Zr}_{10}\text{Cu}_6$	0.21/0.01	0.14/0.01	0.07/0.005	0.05/0.005	0.03/0.004
	$\text{Zr}_7\text{Cu}_9$	0.11/0.007	0.09/0.005	0.05/9.5E-4	0.04/7.0E-4	0.02/0.002
	$\text{Zr}_8\text{Cu}_8$	0.22/0.01	0.16/0.01	0.10/0.01	0.06/0.005	0.04/0.001
	$\text{Zr}_8\text{Cu}_6\text{Al}_2$	0	0.01/8.0E-4	0.05/0.006	0.08/0.007	0.10/0.009
	$\text{Zr}_8\text{Cu}_7\text{Al}_1$	0	0.06/0.006	0.11/0.006	0.11/0.005	0.09/0.005
	$\text{Zr}_9\text{Cu}_6\text{Al}_1$	0	0.07/0.008	0.12/0.01	0.11/0.01	0.08/0.003
	$\text{Zr}_9\text{Cu}_5\text{Al}_2$	0	0.01/0.004	0.04/0.002	0.06/0.004	0.08/0.003
	$\text{Zr}_7\text{Cu}_7\text{Al}_2$	0	0.004/0.001	0.03/0.005	0.04/0.005	0.07/0.005
	$\text{Zr}_7\text{Cu}_8\text{Al}_1$	0	0.03/0.006	0.06/0.005	0.06/0.01	0.06/0.004
	$\text{Zr}_{10}\text{Cu}_5\text{Al}_1$	0	0.04/0.004	0.07/0.01	0.07/0.01	0.07/0.004
	Zr-centered $\langle 0285 \rangle$	$\text{Zr}_{10}\text{Cu}_6$	0.21/0.009	0.17/0.011	0.08/0.004	0.05/0.007
$\text{Zr}_{11}\text{Cu}_5$		0.11/0.008	0.07/0.005	0.03/0.005	0.02/0.004	0.02/0.002
$\text{Zr}_9\text{Cu}_7$		0.28/0.008	0.20/0.009	0.13/0.008	0.09/0.005	0.04/0.004
$\text{Zr}_8\text{Cu}_8$		0.22/0.01	0.16/0.005	0.10/0.007	0.07/0.001	0.04/0.001
$\text{Zr}_7\text{Cu}_9$		0.10/0.004	0.09/0.007	0.05/0.007	0.03/0.002	0.02/0.007
$\text{Zr}_9\text{Cu}_5\text{Al}_2$		0	0.007/0.002	0.04/0.005	0.06/0.001	0.09/0.014
$\text{Zr}_8\text{Cu}_7\text{Al}_1$		0	0.05/0.007	0.10/0.01	0.10/0.01	0.09/0.001
$\text{Zr}_8\text{Cu}_6\text{Al}_2$		0	0.01/0.001	0.04/4.3E-4	0.06/0.001	0.09/0.002
$\text{Zr}_9\text{Cu}_6\text{Al}_1$		0	0.07/0.004	0.11/0.002	0.13/0.006	0.08/0.004
$\text{Zr}_7\text{Cu}_7\text{Al}_2$		0	0.006/0.001	0.03/0.006	0.05/0.007	0.06/0.006
$\text{Zr}_7\text{Cu}_8\text{Al}_1$		0	0.03/0.004	0.06/0.004	0.06/8.5E-4	0.05/0.005
$\text{Zr}_{10}\text{Cu}_5\text{Al}_1$		0	0.04/0.005	0.07/0.003	0.07/0.003	0.06/0.003

**Table 3**Sub-types of Cu-centered  $\langle 00120 \rangle$ ,  $\langle 0281 \rangle$  and  $\langle 0282 \rangle$  in the simulated  $(\text{Cu}_{0.5}\text{Zr}_{0.5})_{100-x}\text{Al}_x$  MGs at 300 K.

VP type	Sub-type	$x=0$	$x=2$	$x=5$	$x=7$	$x=10$
Cu-centered $\langle 00120 \rangle$	Zr <sub>6</sub> Cu <sub>7</sub>	0.28/0.005	0.22/0.004	0.17/0.004	0.13/0.006	0.08/0.003
	Zr <sub>7</sub> Cu <sub>6</sub>	0.29/0.008	0.23/0.003	0.15/0.004	0.11/0.004	0.07/0.002
	Zr <sub>8</sub> Cu <sub>5</sub>	0.18/0.007	0.14/0.003	0.08/0.003	0.05/0.002	0.03/0.001
	Zr <sub>5</sub> Cu <sub>8</sub>	0.14/0.005	0.12/0.003	0.10/0.004	0.07/0.004	0.05/0.003
	Zr <sub>9</sub> Cu <sub>4</sub>	0.05/0.003	0.04/0.003	0.02/0.001	0.01/9.3E-4	0.004/8.7E-4
	Zr <sub>6</sub> Cu <sub>6</sub> Al <sub>1</sub>	0	0.06/0.002	0.10/0.005	0.13/0.005	0.14/0.001
	Zr <sub>5</sub> Cu <sub>7</sub> Al <sub>1</sub>	0	0.03/0.002	0.07/9.3E-4	0.08/0.003	0.10/0.004
	Zr <sub>7</sub> Cu <sub>5</sub> Al <sub>1</sub>	0	0.06/0.003	0.09/0.001	0.10/0.003	0.08/0.002
	Zr <sub>6</sub> Cu <sub>5</sub> Al <sub>2</sub>	0	0.005/9.8E-4	0.02/9.8E-4	0.04/0.002	0.08/0.003
	Zr <sub>5</sub> Cu <sub>6</sub> Al <sub>2</sub>	0	0.002/2.8E-4	0.01/7.8E-4	0.03/9.3E-4	0.06/0.002
Cu-centered $\langle 0281 \rangle$	Zr <sub>7</sub> Cu <sub>5</sub>	0.34/0.01	0.27/0.002	0.19/0.007	0.15/0.001	0.09/0.005
	Zr <sub>8</sub> Cu <sub>4</sub>	0.25/0.009	0.20/0.004	0.13/0.003	0.09/0.005	0.05/0.007
	Zr <sub>6</sub> Cu <sub>6</sub>	0.23/0.006	0.18/0.006	0.14/0.004	0.12/0.009	0.07/0.003
	Zr <sub>5</sub> Cu <sub>7</sub>	0.08/0.004	0.07/0.005	0.05/0.004	0.04/0.006	0.02/0.005
	Zr <sub>9</sub> Cu <sub>3</sub>	0.08/0.001	0.06/0.003	0.04/0.002	0.02/0.003	0.015/0.003
	Zr <sub>7</sub> Cu <sub>4</sub> Al <sub>1</sub>	0	0.06/0.002	0.11/0.005	0.14/0.006	0.12/0.009
	Zr <sub>6</sub> Cu <sub>5</sub> Al <sub>1</sub>	0	0.05/0.005	0.11/0.007	0.13/0.005	0.14/0.007
	Zr <sub>8</sub> Cu <sub>3</sub> Al <sub>1</sub>	0	0.04/0.006	0.05/0.002	0.062/0.003	0.066/0.005
	Zr <sub>6</sub> Cu <sub>4</sub> Al <sub>2</sub>	0	0.006/0.002	0.03/0.002	0.051/0.004	0.10/0.003
	Zr <sub>5</sub> Cu <sub>6</sub> Al <sub>1</sub>	0	0.02/0.003	0.05/0.005	0.05/0.005	0.07/0.004
Cu-centered $\langle 0282 \rangle$	Zr <sub>6</sub> Cu <sub>7</sub>	0.23/0.01	0.21/0.006	0.15/0.01	0.12/0.01	0.09/0.01
	Zr <sub>7</sub> Cu <sub>6</sub>	0.31/0.02	0.25/0.02	0.18/0.006	0.13/0.008	0.08/0.006
	Zr <sub>8</sub> Cu <sub>5</sub>	0.22/0.02	0.15/0.01	0.11/0.006	0.09/0.007	0.04/0.008
	Zr <sub>5</sub> Cu <sub>8</sub>	0.10/0.01	0.09/0.01	0.07/0.005	0.06/0.003	0.05/0.007
	Zr <sub>9</sub> Cu <sub>4</sub>	0.09/0.01	0.05/0.01	0.04/0.003	0.03/0.008	0.02/0.004
	Zr <sub>6</sub> Cu <sub>6</sub> Al <sub>1</sub>	0	0.05/0.004	0.09/0.016	0.13/0.009	0.12/0.007
	Zr <sub>7</sub> Cu <sub>5</sub> Al <sub>1</sub>	0	0.06/0.01	0.09/0.01	0.12/0.007	0.10/0.01
	Zr <sub>6</sub> Cu <sub>5</sub> Al <sub>2</sub>	0	0.002/0.003	0.03/0.003	0.05/8.9E-4	0.09/0.01
	Zr <sub>5</sub> Cu <sub>7</sub> Al <sub>1</sub>	0	0.04/0.004	0.06/0.01	0.066/0.004	0.07/0.007
	Zr <sub>5</sub> Cu <sub>6</sub> Al <sub>2</sub>	0	7.5E-4/1E-4	0.02/0.004	0.04/0.002	0.07/0.01
Zr <sub>7</sub> Cu <sub>4</sub> Al <sub>2</sub>	0	0.003/0.001	0.02/0.008	0.03/0.005	0.05/0.01	

Cu-centered  $\langle 00120 \rangle$ , the Zr<sub>7</sub>Cu<sub>4</sub>Al<sub>1</sub> in Cu-centered  $\langle 0281 \rangle$ , the Zr<sub>7</sub>Cu<sub>5</sub>Al<sub>1</sub> in Cu-centered  $\langle 0282 \rangle$ , the Zr<sub>9</sub>Cu<sub>3</sub>Al<sub>1</sub> and Zr<sub>4</sub>Cu<sub>8</sub>Al<sub>1</sub> in Al-centered  $\langle 00120 \rangle$  and the Zr<sub>5</sub>Cu<sub>8</sub>Al<sub>1</sub> in Al-centered  $\langle 01102 \rangle$  also exhibit similar behaviors upon Al addition. We believe that all the group III sub-types may have close relationship with GFA. A more detailed investigation on the dynamics of these clusters will be very helpful to quantify their contributions to GFA.

### 3.3. Transport properties

The self-diffusion coefficients of the major constituents Zr ( $D_{\text{Zr}}$ ) and Cu ( $D_{\text{Cu}}$ ) in  $(\text{Cu}_{0.5}\text{Zr}_{0.5})_{100-x}\text{Al}_x$  glass-forming liquids as a function of Al contents are depicted in Fig. 7. We selected four representative temperatures upon cooling, namely 1500 K (equilibrium liquid), 1200 K (close to melting temperatures),

1000 K (supercooled liquids) and 800 K (close to glass transition), respectively. The errors bars are derived from the linear fitting using Eq. (6). The self-diffusivities of Al among all the Al-containing compositions are  $3.2 \times 10^{-9}$ ,  $1.3 \times 10^{-9}$ ,  $3.8 \times 10^{-10}$  and  $1.0 \times 10^{-11}$  m<sup>2</sup>/s at 1500, 1200, 1000 and 800 K, respectively. However, the Al self-diffusivities are not present in Fig. 7 since their values are in the limit of the precision accessible by MD simulations. Within the regime of equilibrium liquid at 1500 K, the increasing trend of  $D_{\text{Zr}}$  and  $D_{\text{Cu}}$  upon Al addition can be observed. Approaching the melting temperatures around 1200 K,  $D_{\text{Zr}}$  and  $D_{\text{Cu}}$  still increase upon Al additions. Such Al compositional dependences remain as the melts are further cooled into the supercooled liquid regime at 1000 K. Local minima of  $D_{\text{Zr}}$  and  $D_{\text{Cu}}$  occur around the compositions from  $x=5$  to  $x=7$  at 800 K, which is only about 20–60 K above the glass transition under MD simulations. It is

**Table 4**Sub-types of Al-centered  $\langle 00120 \rangle$  and  $\langle 01102 \rangle$  in the simulated  $(\text{Cu}_{0.5}\text{Zr}_{0.5})_{100-x}\text{Al}_x$  MGs at 300 K.

VP type	Sub-type	$x=2$	$x=5$	$x=7$	$x=10$
Al-centered $\langle 00120 \rangle$	Zr <sub>8</sub> Cu <sub>4</sub> Al <sub>1</sub>	0.31/0.02	0.27/0.01	0.23/0.01	0.19/0.004
	Zr <sub>7</sub> Cu <sub>5</sub> Al <sub>1</sub>	0.25/0.009	0.24/0.006	0.25/0.007	0.20/0.008
	Zr <sub>6</sub> Cu <sub>6</sub> Al <sub>1</sub>	0.19/0.02	0.16/0.009	0.15/0.006	0.17/0.006
	Zr <sub>5</sub> Cu <sub>7</sub> Al <sub>1</sub>	0.09/0.01	0.05/0.005	0.07/0.001	0.07/0.001
	Zr <sub>9</sub> Cu <sub>3</sub> Al <sub>1</sub>	0.10/0.01	0.12/0.008	0.10/0.006	0.10/0.01
	Zr <sub>8</sub> Cu <sub>3</sub> Al <sub>2</sub>	0.003/0.003	0.03/0.003	0.05/0.003	0.053/0.003
	Zr <sub>7</sub> Cu <sub>4</sub> Al <sub>2</sub>	0.001/2E-4	0.03/0.001	0.04/0.006	0.06/0.005
	Zr <sub>6</sub> Cu <sub>5</sub> Al <sub>2</sub>	0.009/0.006	0.02/0.004	0.03/0.006	0.05/0.003
	Zr <sub>4</sub> Cu <sub>8</sub> Al <sub>1</sub>	0.01/0.003	0.007/0.002	0.02/0.002	0.012/0.003
	Al-centered $\langle 01102 \rangle$	Zr <sub>7</sub> Cu <sub>6</sub> Al <sub>1</sub>	0.31/0.02	0.25/0.03	0.24/0.02
Zr <sub>8</sub> Cu <sub>5</sub> Al <sub>1</sub>		0.30/0.02	0.27/0.03	0.25/0.02	0.20/0.03
Zr <sub>9</sub> Cu <sub>4</sub> Al <sub>1</sub>		0.16/0.05	0.12/0.03	0.12/0.01	0.09/0.01
Zr <sub>6</sub> Cu <sub>7</sub> Al <sub>1</sub>		0.13/0.03	0.12/0.02	0.10/0.02	0.11/0.006
Zr <sub>5</sub> Cu <sub>8</sub> Al <sub>1</sub>		0.02/0.004	0.03/0.008	0.042/0.01	0.03/0.01
Zr <sub>7</sub> Cu <sub>5</sub> Al <sub>2</sub>		0.01/0.007	0.06/0.007	0.06/0.01	0.09/0.01
Zr <sub>8</sub> Cu <sub>4</sub> Al <sub>2</sub>		0.04/0.013	0.05/0.01	0.05/0.01	0.07/0.01
Zr <sub>6</sub> Cu <sub>6</sub> Al <sub>2</sub>		0.003/6E-4	0.03/0.008	0.03/0.007	0.07/0.007

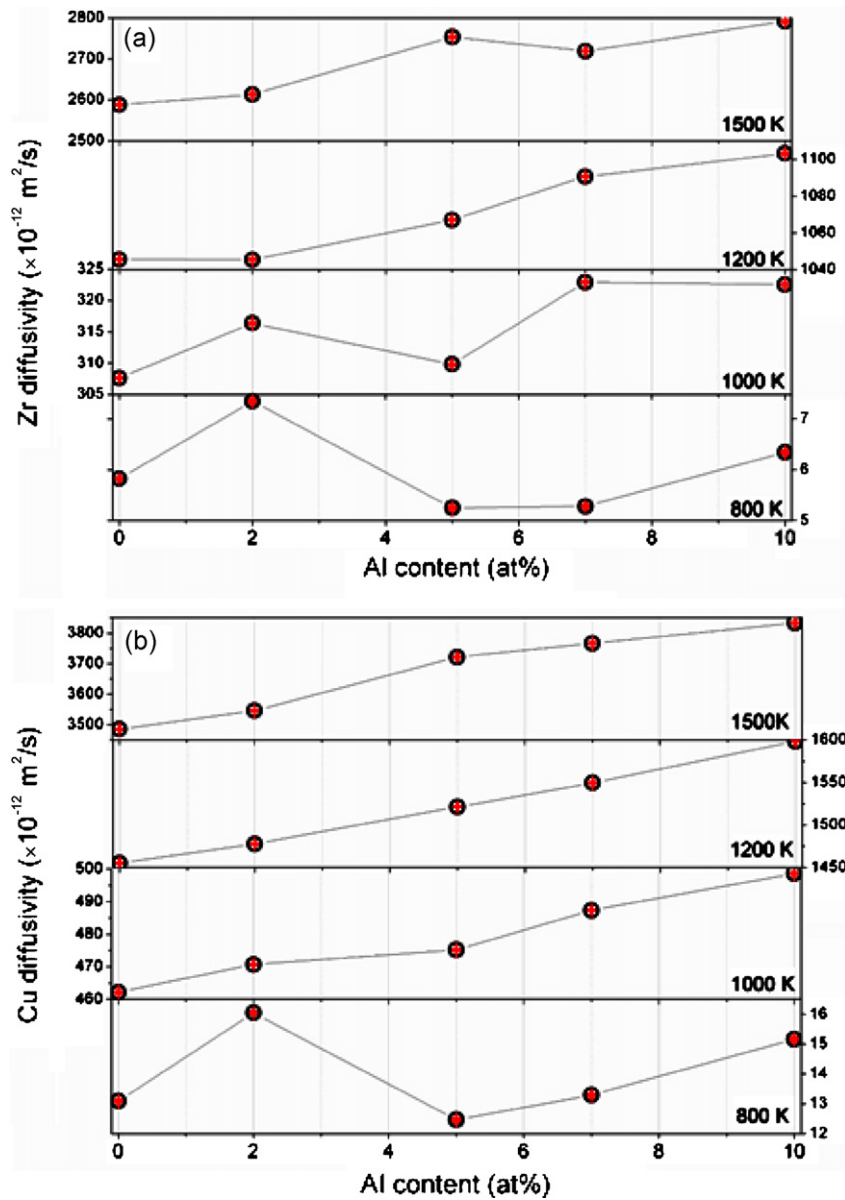


Fig. 7. Self-diffusion coefficients (black circles) and their corresponding errors (red symbols) of (a) Zr and (b) Cu of the simulated  $(\text{Cu}_{0.5}\text{Zr}_{0.5})_{100-x}\text{Al}_x$  liquids at 1500, 1200, 1000 and 800 K, respectively. (For interpretation of the references to color in this figure legend, the reader is referred to the web version of the article.)

believed that the diffusivities of glass-forming liquids around glass transition play a decisive role on the GFA. Such strong dependence of self-diffusivities on Al addition is in excellent agreement with the GFA observed by experiments.

The dependence of self-diffusivities on Al addition can be understood as a cooperation of the following factors: (1) temperature, (2) atomic size and (3) local chemistry environment. In equilibrium liquids, temperature and atomic size have more pronounced effects on diffusivities than local chemistry due to the high kinetic energy. Large atoms such as Zr (Goldschmidt radius 0.160 nm) are hindrance of the movements of other atoms. Therefore, replacing Zr atoms with Al atoms can effectively promote the diffusion of all the elements in  $(\text{Cu}_{0.5}\text{Zr}_{0.5})_{100-x}\text{Al}_x$  liquids. However, in supercooled liquids, the local chemistry will impact the diffusivity more significantly upon undercooling due to the so-called “cage effect” [34]. According to the Stokes law, a diffusive atom with a radius of  $r$  and a velocity of  $v$  experiences a friction force ( $F_f$ ) from the viscous medium,  $F_f = 6\pi r\eta v$ , where  $\eta$  is the viscosity of the medium. It can be deduced from the  $\Delta H_{\text{mix}}$  that Al atoms are more preferable to

cluster with Zr atoms to increase the effective atomic radii. As a consequence, the atomic movements will slow down. We believe that the composition-dependent slow-down of diffusion has close relationship with the group III sub-types clusters identified in Section 3.2.2. However, further investigations are needed to yield a complete understanding of the mechanism behind.

Fig. 8 shows the calculated equilibrium viscosity of the simulated  $(\text{Cu}_{0.5}\text{Zr}_{0.5})_{100-x}\text{Al}_x$  liquids from 2000 to 900 K. For comparison, the viscosity of three Cu–Zr–Al liquids measured by electrostatic levitation is also presented [35]. It can be seen that the viscosity values obtained by MD simulation are comparable with the experimental results. In general, there is no significant dependence of the viscosity of  $(\text{Cu}_{0.5}\text{Zr}_{0.5})_{100-x}\text{Al}_x$  liquids on Al additions from  $x=2$  to 10 in the temperature range from 2000 to 1100 K. The viscosity only decreases slightly with Al contents in from 2000 to 1600 K. However, from 1000 K on, the viscosity of  $x=7$  increases much faster than the other compositions. It can be seen that the viscosity of  $x=7$  is the largest among all the studied compositions at 900 K. Following this trend, it can be deduced

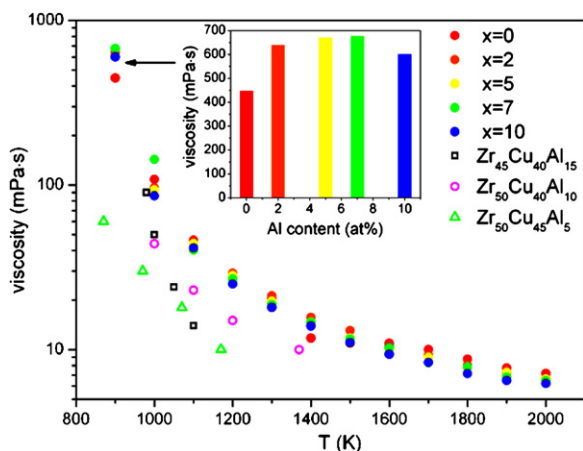


**Fig. 8.** Viscosity of the simulated  $(\text{Cu}_{0.5}\text{Zr}_{0.5})_{100-x}\text{Al}_x$  liquids (solid symbols) from 2000 to 900 K. The open symbols represent the viscosity of three Cu–Zr–Al liquids measured experimentally. The inset shows the dependence of viscosity on Al content at 900 K.

that  $(\text{Cu}_{0.5}\text{Zr}_{0.5})_{100-x}\text{Al}_x$  with  $x = 7$  will increase even faster than all the other studied compositions, although it is difficult to access the equilibrium viscosity below 900 K by MD simulations. It is usually believed that glass-forming liquids with large viscosity in the vicinity of glass transition can slow down the dynamics of the liquids and thus have high glass forming ability. According to the MD simulations, compositions with the best GFA should be close to  $x = 7$ , which is again in good agreement with the experimental results.

#### 4. Conclusions

As a summary, we have performed a systematic investigation on the atomic structures, thermal and transport properties of  $(\text{Cu}_{0.5}\text{Zr}_{0.5})_{100-x}\text{Al}_x$  MGs and liquids with various Al additions using MD simulations, in order to underpin the understanding of the relationship between atomic structures and the experimentally observed GFA in the system. A good correlation between the atomic structures and the GFA has been revealed. Macroscopically, it is found that the composition with  $x = 7$  has the highest viscosity and the lowest diffusivity near the glass transition calculated by MD simulation, which are responsible for and in excellent agreement with the best glass forming composition around  $x = 7$  or 8 determined experimentally. At the atomic scale, the short range order of both MGs and liquids shows a very strong dependence on Al additions. We categorize the sub-types of the ICO and ICO-like clusters into three groups, according to their behaviors upon Al additions.

The group III sub-types, which are ternary clusters mainly with only one substitutive Al atom, show a good correlation with the dependence of viscosity and diffusivity on Al addition. We propose that the group III sub-types play a decisive role on governing the transport properties and GFA in  $(\text{Cu}_{0.5}\text{Zr}_{0.5})_{100-x}\text{Al}_x$  glass-forming liquids.

#### References

- [1] A. Inoue, *Acta Mater.* 48 (2000) 279–306.
- [2] W.H. Wang, C. Dong, C.H. Shek, *Mater. Sci. Eng. R* 44 (2004) 45–89.
- [3] J. Couzin, *Science* 309 (2005) 558.
- [4] H.W. Sheng, W.K. Luo, F.M. Alamgir, J.M. Bai, E. Ma, *Nature* 439 (2006) 419–425.
- [5] G.A. Almyras, C.E. Lekka, N. Mattern, G.A. Evangelakis, *Scr. Mater.* 62 (2010) 33–36.
- [6] G.J. Fan, M. Freels, H. Choo, P.K. Liaw, J.J.Z. Li, W.K. Rhim, W.L. Johnson, P. Yu, W.H. Wang, *Appl. Phys. Lett.* 89 (2006) 241917.
- [7] A. Takeuchi, A. Inoue, *Mater. Trans.* 46 (2005) 2817–2829.
- [8] Y. Li, Q. Guo, J.A. Kalb, C.V. Thompson, *Science* 322 (2008) 1816–1819.
- [9] W.L. Johnson, K. Samwer, *Phys. Rev. Lett.* 95 (2005) 195501.
- [10] J. Das, S. Pauly, C. Duhamel, B.C. Wei, J. Eckert, *J. Mater. Res.* 22 (2007) 326–333.
- [11] Tr. Ananthar, C. Suryanar, *J. Mater. Sci.* 6 (1971) 1111–1135.
- [12] Y.M. Wang, Q. Wang, J.J. Zhao, C. Dong, *Scr. Mater.* 63 (2010) 178–180.
- [13] L. Xia, W.H. Li, S.S. Fang, B.C. Wei, Y.D. Dong, *J. Appl. Phys.* 99 (2006) 026103.
- [14] D. Wang, Y. Li, B.B. Sun, M.L. Sui, K. Lu, E. Ma, *Appl. Phys. Lett.* 84 (2004) 4029–4031.
- [15] Q. Wang, C. Dong, J.B. Qiang, Y.M. Wang, *Mater. Sci. Eng. A: Struct. Mater. Propert. Microstruct. Process.* 449 (2007) 18–23.
- [16] B.W. Zhou, X.G. Zhang, W. Zhang, H. Kimura, T. Zhang, A. Makino, A. Inoue, *Mater. Trans.* 51 (2010) 826–829.
- [17] P. Yu, H.Y. Bai, M.B. Tang, W.L. Wang, *J. Non-Cryst. Solids* 351 (2005) 1328–1332.
- [18] J. Das, M.B. Tang, K.B. Kim, R. Theissmann, F. Baier, W.H. Wang, J. Eckert, *Phys. Rev. Lett.* 94 (2005) 205501.
- [19] P. Yu, H.Y. Bai, *Mater. Sci. Eng. A: Struct. Mater. Propert. Microstruct. Process.* 485 (2008) 1–4.
- [20] T.A. Baser, J. Das, J. Eckert, M. Baricco, *J. Alloys Compd.* 483 (2009) 146–149.
- [21] S. Pauly, S. Gorantla, G. Wang, U. Kuhn, J. Eckert, *Nat. Mater.* 9 (2010) 473–477.
- [22] D.C. Hofmann, *Science* 329 (2010) 1294–1295.
- [23] K. Georgarakis, A.R. Yavari, D.V. Louzguine-Luzgin, J. Antonowicz, M. Stoica, Y. Li, M. Satta, A. LeMoulec, G. Vaughan, A. Inoue, *Appl. Phys. Lett.* 94 (2009) 191912.
- [24] H.Z. Fang, X. Hui, G.L. Chen, Z.K. Liu, *Appl. Phys. Lett.* 94 (2009) 091904.
- [25] Y.Q. Cheng, E. Ma, H.W. Sheng, *Phys. Rev. Lett.* 102 (2009) 245501.
- [26] L. Yang, G.Q. Guo, L.Y. Chen, S.H. Wei, J.Z. Jiang, X.D. Wang, *Scr. Mater.* 63 (2010) 879–882.
- [27] W.G. Hoover, *Phys. Rev. A* 31 (1985) 1695–1697.
- [28] N. Mattern, U. Kuhn, H. Hermann, S. Roth, H. Vinzelberg, J. Eckert, *Mater. Sci. Eng. A: Struct. Mater. Propert. Microstruct. Process.* 375 (2004) 351–354.
- [29] R. Busch, Y.J. Kim, W.L. Johnson, *J. Appl. Phys.* 77 (1995) 4039–4043.
- [30] N. Mattern, P. Jovari, I. Kaban, S. Gruner, A. Elsner, V. Kokotin, H. Franz, B. Beuneu, J. Eckert, *J. Alloys Compd.* 485 (2009) 163–169.
- [31] X. Hui, H.Z. Fang, G.L. Chen, S.L. Shang, Y. Wang, J.Y. Qin, Z.K. Liu, *Acta Mater.* 57 (2009) 376–391.
- [32] S.G. Hao, C.Z. Wang, M.J. Kramer, K.M. Ho, *J. Appl. Phys.* 107 (2010) 053511.
- [33] S.Q. Wu, C.Z. Wang, S.G. Hao, Z.Z. Zhu, K.M. Ho, *Appl. Phys. Lett.* 97 (2010) 021901.
- [34] D. Turnbull, M.H. Cohen, *J. Chem. Phys.* 52 (1970) 3038–3041.
- [35] Y. Yokoyama, T. Ishikawa, J.T. Okada, Y. Watanabe, S. Nanao, A. Inoue, *J. Non-Cryst. Solids* 355 (2009) 317–322.